SUPLEMENTARY MATERIALS for Chubykin et al.: "Activity-Dependent Validation of Excitatory vs. Inhibitory Synapses by Neuroligin-1 vs. Neuroligin-2"

SUPPLEMENTARY TEXT

We analyzed EPSCs in acute slices and in cultured neurons prepared from littermate wild-type and NL1 KO mice to test whether the deletion of NL1 alone would induce a change in synaptic strength. However, we found that the NL1 deletion had no effect on EPSC size in slices or in dissociated cultures. To test whether this result occurs because the amount of synaptic network activity is insufficient to reveal a contribution of endogenous NL1 to activity-dependent synapse modulation, we investigated the effect of chronic treatments with picrotoxin (to activate spontaneous EPSCs), AP5, or a combination of picrotoxin and AP5 on EPSCs in cultured neurons (Suppl. Fig. 7). The chronic picrotoxin treatment in this experiment is expected to enhance the excitatory drive in the culture, which might reveal differences between NL-1 KO and wild-type neurons as a function of AP5. However, we observed no differences between wild-type and KO neurons, disproving this hypothesis.

SUPPLEMENTARY METHODS

Constructs. All NL1 expression vectors encode rat NL1 with inserts in splices sites A and B (Biederer et al., 2002; Sara et al., 2005). pCMV5-NL1 encodes full-length rat NL1 containing splice sites A and B. Generated by cloning the NL1 cDNA into the Bgl II/Sal I sites of pCMV5. pCMV5-NL1-EGFP encodes full-length rat NL1. Generated by cloning a PCR fragment containing the coding sequence of EGFP into the Rsr II site of pCMV5-NL1. pNL1-ΔC-EGFP encodes rat NL1, truncated at Rsr II site after the codon corresponding to T776 and fused to EGFP followed by a stop codon. It was generated from pCMV5-NL1-EGFP by cloning the Bgl II/BsrGI fragment of NL1-EGFP into the Bgl II/BsrGI sites of EGFP-N1 (Clontech). pcDNA3-AchE-NL1-EGFP generated by replacing extracellular part of NL1 ending with H634 with mouse AchE truncated at L539. Afl II sites were introduced in mouse AchE after the codon corresponding to L539 and in rat NL1 before the codon corresponding to H634 using QuickChange site directed mutagenesis (Stratagene). Subsequently, C-terminal part of NL1 was cloned into the Afl II/Xba I sites of pcDNA3-AchE. EGFP fusion was created by cloning a PCR fragment containing the coding sequence of EGFP into the Rsr II site of pcDNA3-AchE-NL1 (Chubykin et al., 2005). pCMV5-NL1-R473C-EGFP encodes mutant NL1 with R473C mutation corresponding to human NL3 R451C autism mutation. Generated by QuickChange site directed mutagenesis (Stratagene) using rat NL1 as a template. EGFP fusion was created by cloning a PCR fragment containing the coding sequence of EGFP into the Rsr II site of pCMV5-NL1-R473C. pCMV5-NL2-Venus encodes full-length rat NL2. PCR fragment containing the

coding sequence of Venus was cloned into the RsrII site, which was introduced in rat NL2 after the codon corresponding to L762 using QuickChange site directed mutagenesis (Stratagene). pPDGF-EGFP-β-Actin encoding EGFP-tagged full-length β-Actin, was kindly provided by Y.Goda (University College, London, UK)(Morales et al., 2000). pCMV5-SynCAM encodes full-length mouse SynCAM cloned into EcoRI site of pCMV5(Biederer et al., 2002). pCMV5-SynCAM-NL1-IRES-ECFP encodes extracellular part of SynCAM fused to C-terminal part of NL1(Sara et al., 2005) . pCMV5-NL1-SynCAM-IRES-ECFP encodes extracellular part of NL1 fused to C-terminal part of SynCAM(Sara et al., 2005).

Electrophysiological analyses of NL1 KO mice were performed in acute hippocampal and cortical slices at room temperature (~22 °C) from littermate mice that were either homozygous NL1 KO mice, or contained one or two wild-type NL1 alleles. All recordings were performed in standard artificial cerebrospinal fluid containing (in mM): 126 NaCl, 3 KCl, 1.25 NaH_2PO_4, 2 $MgSO_4$, 26 $NaHCO_3$, 10 dextrose, and 2 $CaCl_2$, and saturated with 95% O_2/5% CO_2 (final pH of 7.4). The pipette solution for the whole-cell recordings contained (in mM): 125 Cs-methanesulfonate, 1 CsCl, 3 NaCl, 10 HEPES-NaOH pH 7.25, 2.5 BAPTA, 4 ATP-Mg, 0.3 GTP-Tris, 14 phosphocreatine-Tris, 10 sucrose (290 mOsm); in all recordings, seals with a series resistance of >13 MΩ were excluded. Two types of experiments were performed: 1. Measurements of EPSCs. Whole-cell recordings were performed from CA1 pyramidal neurons in slices from mice at P19-21 in the presence of 100 μM picrotoxin to prevent disynaptic inhibitory responses. Most of the CA3 region was removed to prevent polysynaptic responses. An extracellular stimulating electrode (2 cond. cluster electrode, FHS, Bowdoin, Maine) was positioned in the stratum radiatum ~75 μm away from the patched neuron. Measurements were then performed in four stages: a. We first tested whether extracellular stimulation produced monosynaptic responses using a holding potential of -70 mV and approximately -30 mV to ensure that disynaptic inhibitory responses did not occur; b. we then optimized the stimulation strength to elicit AMPA-receptor mediated responses of -50 to -100 pA (current pulses used were 50-400 μA); c. using this stimulus strength, we measured AMPA responses in 5-10 stimuli applied at 0.125 Hz with a postsynaptic holding potential of -70 mV; and d. finally, we measured postsynaptic NMDA-receptor mediated responses in the same cell by switching the postsynaptic holding potential to +40 mV. AMPA-mediated responses were monitored as the peak amplitude; NMDA-receptor mediated responses as the amplitude 40 ms after the stimulus to ensure that only NMDA-receptor dependent currents were measured. Moreover, in two experiments AP5 was shown to completely block the measured NMDA-receptor dependent currents, validating the measurements. 2. Measurements of IPSCs were performed in paired recordings in layer 4 of the somatosensory cortex (within barrel hollows) in acute slices obtained from P14-16 mice. Whole-cell recordings were established in neighboring presynaptic inhibitory fast-spiking and postsynaptic regular-spiking neurons (interior pipette solution: (mM): 130 K-methanesulfonate, 3 KCl, 1 NaCl, 10 HEPES-NaOH pH 7.25, 0.1 EGTA, 4 ATP-Mg, 0.3 GTP-Tris, 14 phosphocreatine-Tris, 10 sucrose (290 mOsm). Of 24 patched wild-type pairs, 12 had inhibitory connections

and 17 had excitatory connections; of 20 patched NL1 KO pairs, 10 had inhibitory connections and 15 excitatory connections; no presumptive inhibitory neuron ever elicited an EPSC, and no presumptive excitatory neuron an IPSC. This together with the previous literature suggests that the vast majority of postsynaptic neurons were excitatory stellate neurons, and the fast-spiking presynaptic neurons neocortical inhibitory neurons (Gibson et al., 1999). Recordings were in voltage clamp with the presynaptic fast-spiking neuron held at -60 mV and the postsynaptic excitatory neuron held at -55 mV. Reversal for IPSCs were ~-75 mV. Junction potentials were 9 mV. IPSCs were measured in response to a 20 Hz stimulus train of 8 evoked presynaptic action potentials, and the absolute amplitude and short-term synaptic plasticity of responses were measured. The failure rate of unitary IPSCs was 9 ± 3% for wild-type slices (n=12), and 6 ± 4% for NL1 KO slices (n=10; data are means ± SEMs; p=0.57).

Immunocytochemistry, image acquisition and analysis. Neurons were fixed in cold 100% methanol, permeabilized in 0.1% saponin, and incubated with primary and secondary antibodies in PBS with 3% nonfat milk and 0.1% saponin. Immunolabeling of presynaptic terminals and of dendrites was performed with rabbit polyclonal antibodies to synapsin (E028)(Rosahl et al., 1993) and mouse monoclonal antibodies to MAP2 (Sigma Aldrich), respectively, using Alexa Fluor 633 goat anti-rabbit and Alexa Fluor 546 goat anti-mouse antibodies (Molecular Probes) as secondary antibodies. Images were acquired with a 63x objective using a 4.5x zoom in a Leica TCS2 conlocal microscope with identical settings applied to all samples in an experiment. Images were presented in three colors: presynaptic terminals were visualized via synapsin staining represented in red channel, dendrites via MAP2 staining in blue channel, and spines via the EGFP fluorescence (either from the transfected EGFP-tagged NL1 proteins or from co-transfected EGFP-tagged β-actin). Stacks of z-section images were converted to maximal projection images and analyzed blindly with the NIH Image/ImageJ program. Channels corresponding to EGFP and synapsin signals were thresholded to outline spines and presynaptic terminals correspondingly. Area size, fluorescent intensity and density of spines and presynaptic terminals per 50 μm of dendrite were measured using the "Analyze particle" module of the ImageJ program. All samples were coded and analyzed blindly. Each experiment was performed at least three times with 300-1000 spines from 6 to 10 neurons analyzed per condition.

References

Boucard, A. A., Chubykin, A. A., Comoletti, D., Taylor, P., and Sudhof, T. C. (2005). A Splice Code for trans-Synaptic Cell Adhesion Mediated by Binding of NL1 to alpha- and beta-Neurexins. Neuron *48*, 229-236.

Chih, B., Afridi, S. K., Clark, L., and Scheiffele, P. (2004). Disorder-associated mutations lead to functional inactivation of neuroligins. Hum Mol Genet *13*, 1471-1477.

Chih, B., Engelman, H., and Scheiffele, P. (2005). Control of excitatory and inhibitory synapse formation by neuroligins. Science *307*, 1324-1328.

Dean, C., Scholl, F. G., Choih, J., DeMaria, S., Berger, J., Isacoff, E., and Scheiffele, P. (2003). Neurexin mediates the assembly of presynaptic terminals. Nat Neurosci *6*, 708-716.

Dresbach, T., Neeb, A., Meyer, G., Gundelfinger, E. D., and Brose, N. (2004). Synaptic targeting of neuroligin is independent of neurexin and SAP90/PSD95 binding. Mol Cell Neurosci *27*, 227-235.

Graf, E. R., Zhang, X., Jin, S. X., Linhoff, M. W., and Craig, A. M. (2004). Neurexins induce differentiation of GABA and glutamate postsynaptic specializations via neuroligins. Cell *119*, 1013-1026.

Iida, J., Hirabayashi, S., Sato, Y., and Hata, Y. (2004). Synaptic scaffolding molecule is involved in the synaptic clustering of neuroligin. Mol Cell Neurosci *27*, 497-508.

Levinson, J. N., Chery, N., Huang, K., Wong, T. P., Gerrow, K., Kang, R., Prange, O., Wang, Y. T., and El-Husseini, A. (2005). Neuroligins mediate excitatory and inhibitory synapse formation: involvement of PSD-95 and neurexin-1beta in neuroligin-induced synaptic specificity. J Biol Chem *280*, 17312-17319.

Nam, C. I., and Chen, L. (2005). Postsynaptic assembly induced by neurexin-neuroligin interaction and neurotransmitter. Proc Natl Acad Sci U S A *102*, 6137-6142.

Prange, O., Wong, T. P., Gerrow, K., Wang, Y. T., and El-Husseini, A. (2004). A balance between excitatory and inhibitory synapses is controlled by PSD-95 and neuroligin. Proc Natl Acad Sci U S A *101*, 13915-13920.

Sara, Y., Biederer, T., Atasoy, D., Chubykin, A., Mozhayeva, M. G., Sudhof, T. C., and Kavalali, E. T. (2005). Selective capability of SynCAM and neuroligin for functional synapse assembly. J Neurosci *25*, 260-270.

Supplementary Table 1

Summary of previous morphological and electrophysiological studies of neuroligins in transfected neurons

Publication	Target protein	Immunocytochemistry	Electrophysiology
Dean et al., 2003	Transfection NL1	NL1 increases density of synapsin, PSD-95 and GluR2/3 puncta	Not tested
Chih et al., 2004	Transfection NL3, NL4, NL3 R451C, NL4 D396X	NL3, NL4 increase synapse density; NL4 D396X has no effect, NL3 R451C has no effect, except in some cells with high level of expression where synapse density is increased	Not tested
Dresbach et al., 2004	Transfection NL1, NL1ΔC	NL1 is targeted to dendritic spines via its C-terminal sequence; NL1ΔC mutant lacking C-tail is not localized in spines	Not tested
Graf et al., 2004	Transfection NL1, NL2, NL3, NL4	NL1, NL3, NL4 clusters PSD-95, NL2 clusters gephyrin, PSD-95	NL2 decreases frequency and amplitude of mEPSCs and mIPSCs
Iida et al., 2004	Transfection NL1, NL1+S-SCAM, NL1+PSD-95, NL1-C, NL1-C-del	Co-transfection with S-SCAM, but not with PSD-95 clusters NL1 in spines; NL1 induces transient increase in density of synaptophysin puncta	Not tested
Prange et al., 2004	Transfection NL1, NL1+PSD-95; siRNA PSD-95	NL1 increases VGLUT and VGAT clusters density; co-transfection with PSD-95 restricts NL1 localization to excitatory synapses	NL1 increases mEPSC and mIPSC frequency, and mEPSC amplitude; co-transfection of PSD-95 with NL1 abolishes mIPSC effect and enhances mEPSC effect

Boucard et al., 2005	Transfection NL1, NL1ΔAB	NL1 increases synapse density; NL1ΔAB less efficiently increases synapse density and increases synapse size	Not tested
Chih et al., 2005	Transfection NL1, NL2, NL3, NL1swap, NL1ΔC mutants; shRNA sh-NL1, NL2, NL3, sh-NL1+NL2+NL3	NL1 increases density of PSD-95, Homer, NR1 and VGlut1 puncta; NL2, NL3 increase density of VGlut1 and VGAT puncta; NL1swap increases density of PSD-95, but not NR1 puncta, NL1ΔC increases density of NR1, but not PSD-95 puncta; sh-NL1,2,3, sh-NL1+NL2+NL3 decrease density of spines and VGlut1, GluR1 puncta	sh-NL1+2+3 'knockdown' of all three neuroligins decreases mIPSC frequency and amplitude, and slightly decreases the mEPSC amplitude
Levinson et al., 2005	Transfection NL1, NL2, NL3, NL2+PSD-95, NL3+PSD-95	NL1, NL2, NL3 increase VGLUT and VGAT clusters density; PSD-95 shifts NL2 localization from inhibitory to excitatory synapses	NL1 increases mEPSCs and mIPSCs frequency and amplitude; this effect is blocked by soluble Nrx-Fc
Nam et al., 2005	Transfection NL1, NL1ΔC mutant	NL1ΔC reduces clustering of PSD-95 and AMPA receptors; NL1 is not tested	NL1ΔC decreases AMPA mEPSCs frequency and amplitude, and NMDA sEPSCs amplitude; NL1 is not tested
Sara et al., 2005	Transfection NL1, SynCAM	NL1 increases synapse density in immature neurons; SynCAM has no effect	SynCAM increases mEPSCs frequency in immature neurons; NL1 has no effect

Supplementary Table 2

Statistical analysis of the relative effect of chronic AP5 treatment on synaptic responses and synapse numbers in control-transfected and NL1-transfected neurons

Figure	Transfection	Analysis	Ratio AP5	Statistical Significance	
			untreated/ treated +/- SER*	AP5 treatment	NL vs. Control Transfection
1	NL1-EGFP	AMPA EPSCs	1.9+/-0.2	p<0.01	p<0.01
	EGFP		1.6+/-0.3	p<0.05	
	NL1-EGFP	NMDA EPSCs	2.9+/-0.4	p<0.01	p<0.01
	EGFP		1.7+/-0.4	p<0.05	
	NL1-EGFP	N/A EPSCs	1.7+/-0.3	p<0.01	p<0.01
	EGFP		1.1+/-0.2	ns	
	NL1-EGFP	Spine Density	1.9+/-0.3	p<0.01	p<0.01
	EGFP		1.5+/-0.3	ns	
	NL1-EGFP	Synapse Density	2.2+/-0.5	p<0.01	p<0.01
	EGFP		1.6+/-0.4	p<0.05	
5	NL2-Venus	AMPA EPSCs	1.1+/-0.2	ns	ns
	EGFP		1.4+/-0.3	ns	
	NL2-Venus	NMDA EPSCs	1.4+/-0.3	ns	ns
	EGFP		1.5+/-0.3	p<0.05	
	NL2-Venus	N/A EPSCs	1.1+/-0.2	ns	ns
	EGFP		1.2+/-0.3	ns	
	NL2-Venus	Spine Density	0.8+/-0.2	ns	p<0.05
	EGFP		1.15+/-0.14	ns	
	NL2-Venus	Synapse Density	1.3+/-0.3	ns	ns
	EGFP		1.1+/-0.3	ns	

S1	NL1	AMPA EPSCs	2.6+/-0.3	p<0.01	p<0.01
	SynCAM		1.2+-0.2	ns	
	NL1	NMDA EPSCs	3.2+/-0.5	p<0.01	p<0.01
	SynCAM		1.3+/-0.3	ns	
	NL1	N/A EPSCs	1.4+/-0.3	ns	p<0.01
	SynCAM		1.1+/-0.3	ns	
	NL1	Spine Density	1.9+/-0.3	p<0.01	p<0.01
	SynCAM		1.4+/-0.5	ns	
	NL1	Synapse Density	1.8+/-0.3	p<0.01	p<0.01
	SynCAM		1.6+/-0.5	p<0.05	
S2	NL1-EGFP	Spine Density	1.8+/-0.3	p<0.01	p<0.01
	EGFP-actin		0.88+/-0.12	ns	
	NL1-EGFP	Synapse Density	1.6+/-0.2	p<0.01	p<0.01
	EGFP-actin		1.1+/-0.2	ns	
	NL1-EGFP	Inhibitory Synapse Density	1.0+/-0.3	ns	ns
	EGFP-actin		0.8+/-0.2	ns	

*SER (σR)– statistical error of ratios is defined by a formula: $\sigma R = R \bullet \sqrt{\left(\frac{\sigma f}{f}\right)^2 + \left(\frac{\sigma g}{g}\right)^2}$, where R=f/g, f is untreated condition, g is treated condition. The ratios represent untreated/treated conditions for different constructs in corresponding figures 1,5,S1,S2. Standard error of the ratio untreated/treated was calculated using the formula:

$$SEM_{untreated/treated} = \frac{untreated}{treated}\sqrt{\left(\frac{SEM_{untreated}}{untreated}\right)^2 + \left(\frac{SEM_{treated}}{treated}\right)^2}$$

$SEM_{untreated}$ and $SEM_{treated}$ represent corresponding SEMs for untreated and treated condition. This standard formula recalculates the SEM of a ratio based on known means and SEMs of the components of this ratio. Thus, for example the first value in the Ratio AP5 column represents the ratio of the mean AMPA EPSC of the NL1-EGFP-transfected neurons not treated with AP5 divided by the mean AMPA EPSC of the NL1-EGFP-transfected neurons treated with AP5. This ratio is 1.9. In order to calculate this ratio, we took the mean values for AMPA EPSCs for NL1-EGFP and NL1-EGFP+AP5 determined before. They were determined as the average values of the 3 mean AMPA EPSCs of 3 different experiments. The SEMs of these values were determined as a square root of the sum of the squares of the SEMs of the individual experiments. The SEM of the ratio, which is called SER here, is calculated by the formula above and equals 0.2 (the rounding of the SEMs is performed to the first meaningful digit if it is ≥ 15 (if it is <15, we leave 2

digits). The rounding of the SEMs determines the rounding of the ratio, so we have the ratio equals 1.9 and the error 0.2. So, we represent it as 1.9+/- 0.2. The p-value for the AP5 treatment represents the p-value for the student t-test for comparison of statistical difference between AMPA EPSCs of NL1-EGFP-transfected neurons and AMPA EPSCs of NL1-EGFP-transfected neurons and treated with AP5. The next p-value of transfection represents the p-value for the student t-test for comparison of statistical difference between AMPA EPSCs of NL1-EGFP-transfected neurons and AMPA EPSCs of EGFP-transfected neurons.
And the next row is the same procedure for AMPA EPSCs of EGFP-transfected neurons, and so on.

SUPPLEMENTARY FIGURE LEGENDS

Supplementary Figure 1

Differential effect of chronic AP5 treatment on synapse numbers and synaptic transmission in neurons expressing NL1 or SynCAM. **(A)** Images of neurons co-transfected with EGFP-β-actin and NL1 or SynCAM, with or without chronic AP5 treatment. Every condition is represented by two images: the left image displays the EGFP fluorescence used to visualize dendritic spines and filopodia (green), and the right image the merged pictures of the EGFP fluorescence (green) and of immunocytochemistry for MAP2 (blue) and synapsin (red). **(B)** and **(C)** Summary graphs of the effects of chronic blockade of NMDA receptors with AP5 on synapse numbers (B) and size (C). **(D)** Representative traces of evoked NMDA and AMPA receptor-dependent EPSCs in neurons co-transfected with EGFP and NL1 or SynCAM, with or without AP5 treatment. **(E)** Mean amplitudes of NMDA and AMPA receptor-dependent EPSCs and mean NMDA/AMPA ratios of neurons expressing NL1 or SynCAM without or with chronic AP5 treatment. Data shown in panels (B), (C), and (E) are means ± SEMs (3 experiments, n=18 cells for each sample); statistical significance of the effect of AP5 treatment was evaluated with the Student's t-test; asterisks represent statistical significance of difference between SynCAM and SynCAM+AP5, SynCAM and NL1, NL1 and NL1+AP5 (* = $p<0.05$; ** = $p<0.01$; ns = not significantly different).

Supplementary Figure 2

Effect of NL1 and of chronic blockade of NMDA receptors on inhibitory synapse numbers. **(A)** Representative images of hippocampal neurons transfected with EGFP-actin or NL1-EGFP cultured in the presence or absence of 50 μM AP5 for four days. Neurons were visualized by EGFP fluorescence (green), and immunolabeling with antibodies to the vesicular GABA transporter (VGAT) (blue) and to the presynaptic marker synapsin (red). For each sample, the red synapsin and the blue VGAT channels, as well as the merged image of all three channels are shown. **(B)** and **(C)** Summary graphs of the quantitative analysis of synapse numbers (B) and size (C) in neurons expressing EGFP-actin, or EGFP-tagged NL1, and treated with either control medium or AP5 (n=3 independent experiments with 8 neurons/experiment and condition); asterisks represent statistical significance of difference between EGFP and EGFP+AP5, NL1-EGFP and NL1-EGFP+AP5 (Student's t-test; * = $p<0.05$; ** = $p<0.01$).

Supplementary Figure 3

NL2 expression in hippocampal neurons. Representative images of neurons expressing EGFP or NL2-Venus. Image acquisition was done using GFP filter in both cases of EGFP and NL2-Venus. Every condition is represented by two images: the left image displays the EGFP fluorescence (green), and the right image the merged pictures of the EGFP fluorescence (green) and of immunocytochemistry for MAP2 (blue) and synapsin (red). Calibration bar in left panels applies to all panels.

Supplementary Figure 4

EPSC input/output curves in cortical slices from NL1 and NL2 KO mice. Evoked EPSCs were measured in Layer 2/3 of the somatosensory (barrel) cortex in response to extracellular stimulation in Layer 2/3, with 1-2 cells/slice analyzed in order to minimize epileptiform activity. **(A)** and **(B)** Representative traces and summary graph for evoked EPSCs for NL1 KO mice and wild type littermate pairs (n=2). **(C)** and **(D)** Representative traces and summary graph for evoked EPSCs for NL2 KO mice and wild type littermate pairs (n=3). Note that network activity predominated at low stimulus strengths, and that to exclude its effect, the initial peak in the trace was taken as the evoked response (indicated by arrow). Data shown in (B), and (D) are means ± SEMs; asterisks indicate statistically significant differences (** = $p<0.01$; *** = $p<0.001$).

Supplementary Figure 5

Effect of NL1 mutations on neuronal synapse density. **(A)** Diagram of constructs used for transfections. **(B)** Morphological analysis of transfected neurons. Representative examples of merged EGFP-, MAP2- and synapsin-localizations (green, blue and red correspondingly) in neurons transfected with EGFP alone, with the EGFP-tagged NL1 (NL1-EGFP), with the acetylcholinesterase/NL1 fusion protein (AchE-NL1-EGFP) or with the R473C-mutant NL1 ($NL1^{R473C}$-EGFP). Calibration bar in the left panel applies to all panels. **(C)** and **(D)** Summary graphs of the effect of expressing the various NL1 proteins on synapse number (B) and size (C). Density and size of spines and presynaptic terminals on a dendrite, determined from the EGFP-fluorescence or synapsin-localization data. Data shown are means ± SEMs (n=3 independent experiments with 6-10 neurons/experiment and condition); asterisks indicate that a sample is significantly different from the EGFP-only transfected control (Student's t-test; * = $p<0.05$; ** = $p<0.01$).

Supplementary Figure 6

Morphological analysis of the effect of the overexpression of NL/SynCAM chimeras on synapses. Comparative analysis of the effects of NL1, SynCAM, and NL1/SynCAM chimeras on synapse numbers in hippocampal neurons. Neurons were co-transfected with the indicated constructs **(A)** and EGFP-β-actin and analyzed for spine and synapse density and size. **(B)** Representative images of hippocampal neurons co-transfected with neuroligin 1 and EGFP-β-actin, and visualized by virtue of the EGFP-actin fluorescence and synapsin immunocytochemistry (red). Image on right shows the merged view of both fluorescence pictures. **(C)** Merged images of neurons co-transfected with SynCAM, NL1-SynCAM, or SynCAM-NL1 and EGFP-actin. **(D)** and **(E)** Summary graphs of the density (C) and sizes (D) of postsynaptic spines and presynaptic terminals. Data shown are means ± SEMs (n=20 cells in 3 experiments for each sample); significance was evaluated by the Student's t-test ; asterisks represent statistical significance of difference between SynCAM and NL1, NL1-SynCAM and SynCAM-NL1 (* = $p<0.05$; ** = $p<0.01$; ns = not significantly different; all relative to the SynCAM-transfected sample).

Supplementary Figure 7

Electrophysiological analysis of the effect of the overexpression of NL/SynCAM chimeras on synapses. **(A)** Representative traces of NMDA- (top) and AMPA-receptor (bottom) dependent EPSCs. **(B)** Amplitudes of NMDA- and AMPA-receptor dependent EPSCs and NMDA/AMPA ratios of neurons co-transfected with NL1, SynCAM, NL1-SynCAM, or SynCAM-NL1 and EGFP-β-actin. Data shown are means ± SEMs (n=18); asterisks indicate whether a result is significantly different between the samples in the pairs of NL1 and SynCAM, NL1-SynCAM and SynCAM-NL1, NL1 and NL1-SynCAM, SynCAM and SynCAM-NL1 (Student's t-test; * = $p<0.05$; ** = $p<0.01$; ns = not significantly different).

Supplementary Figure 8

Effect of chronic picrotoxin (PTX) and AP5 treatments on AMPA- and NMDA-receptor mediated EPSC amplitudes in cultured neurons from wild-type and NL1-KO mice. **(A)** and **(B)**, and **(C)** and **(D).** Sample traces (A and C) and summary graphs (B and D) of AMPA-EPSCs (A and B) and NMDA-EPSCs (C and D). Cultured neurons were prepared from newborn NL1-KO or littermates control mice, and incubated in 50 μM AP5 ± 10 μM CNQX and 50 μM PTX at DIV-10 to block all activity; recordings were performed at 14-15 DIV. EPSCs were measured in 50 μM PTX at a -70 mV (A and B) or +40 mV holding potential (C and D). AP5 or AP5 + PTX treatment significantly reduced AMPA-EPSC size in wildtype neurons but not in NL1-KO neurons. [For B: Wild type: Mock treated = 1608.86 ± 116.78 pA, n = 22; PTX treated = 1504.5 ± 116.96 pA, n = 21; AP5 = 1266.17 ± 89.76 pA, (p = 0.032) n = 20; AP5 + PTX treated = 1252.64 ± 121 pA, (p = 0.043) n = 20; NL1 knock-out: Mock treated = 1546.38 ± 145.45 pA, n = 18; PTX treated = 1541.25 ± 113.7 pA, n = 16; AP5 = 1405. 7 ± 91.9 pA, n = 14; AP5 + PTX treated = 1350.33 ± 133.76 pA, n = 16. For D: Wild type: Mock treated = 721.13 ± 63.9 pA, n = 22; PTX treated = 797.5 ± 62.8 pA, n = 21; AP5 = 500.88 ± 39.7 pA, (p = 0.009) n = 20; AP5 + PTX treated = 492.64 ± 42,3 pA, (p = 0.0082) n = 20; NL1 knock-out: Mock treated = 642.5 ± 64.48 pA, n = 18; PTX treated = 676.25 ± 69.09 pA, n = 16; AP5 = 554.64 ± 46.9 pA, n = 14; AP5 + PTX treated = 615.66 ± 73.8 pA, n = 16]

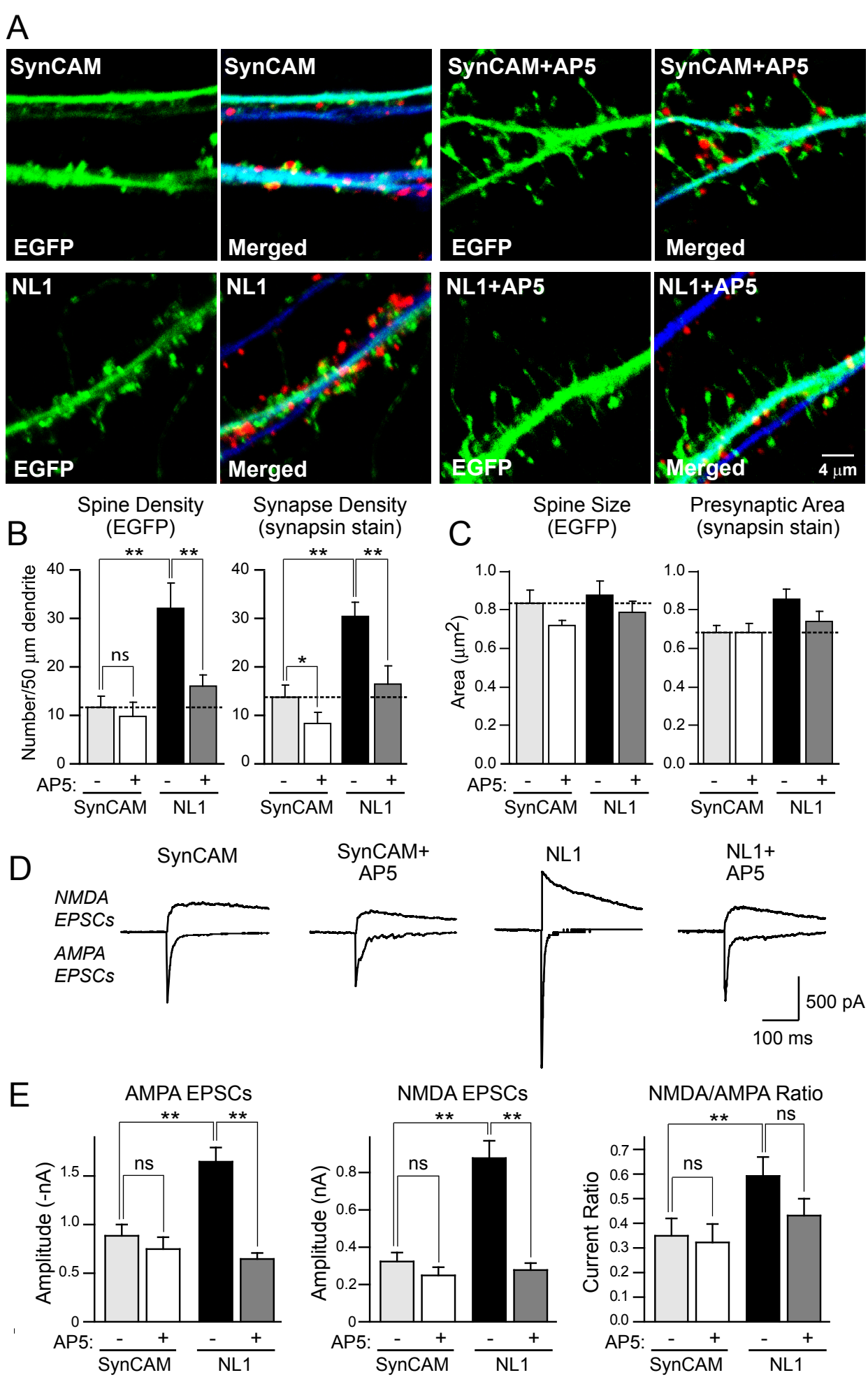

Supplementary Figure 1
Chubykin et al.

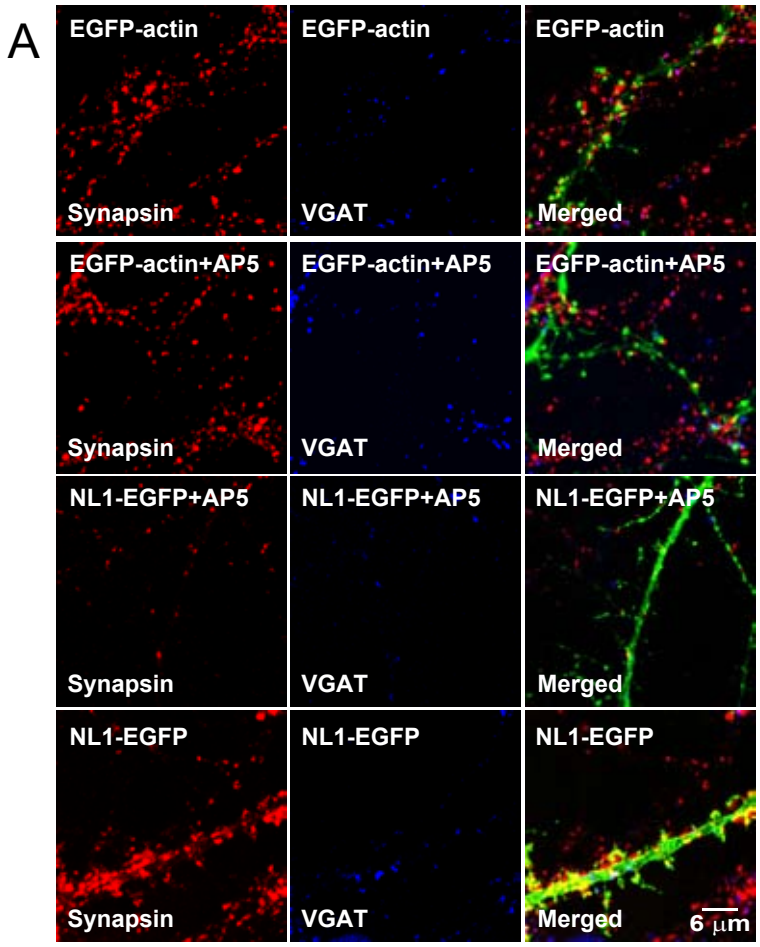

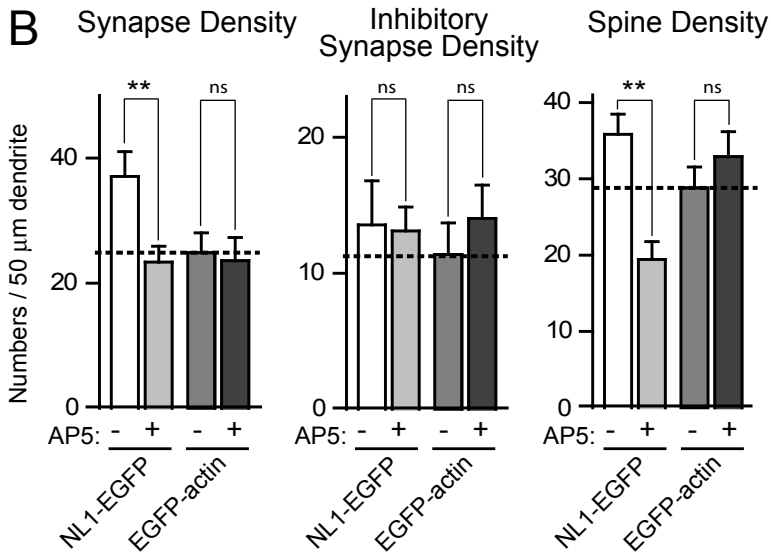

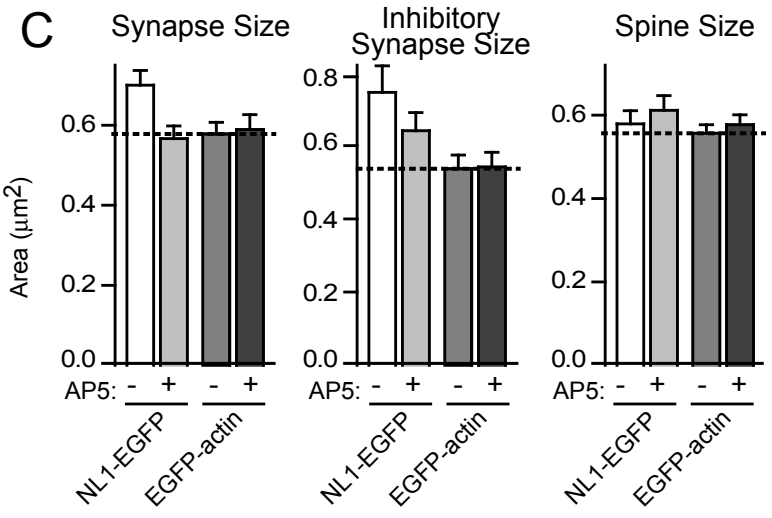

Supplementary Figure 2
Chubykin et al.

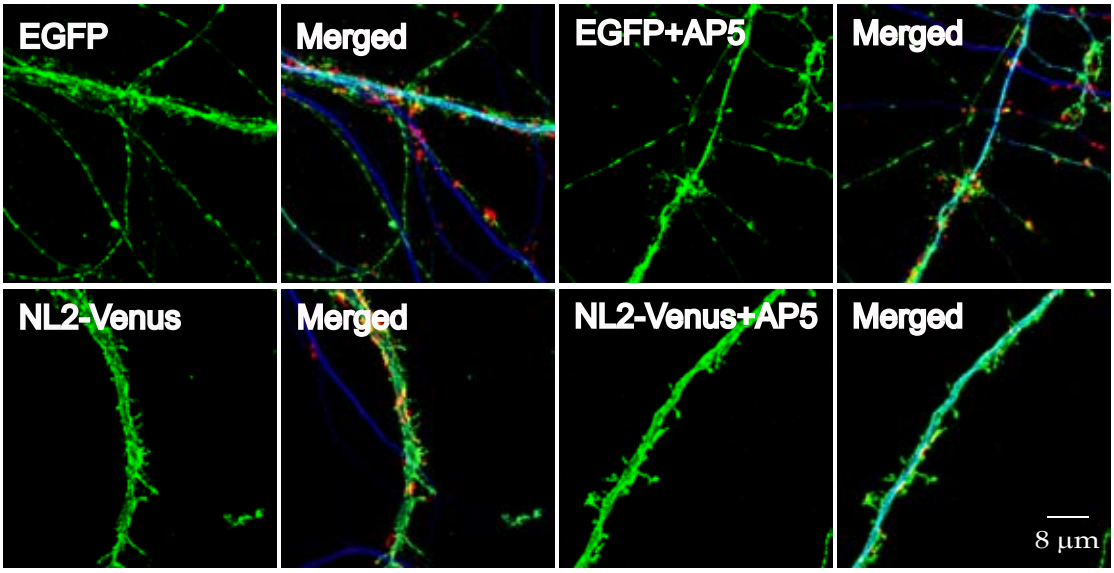

Supplementary Figure 3
Chubykin et al.

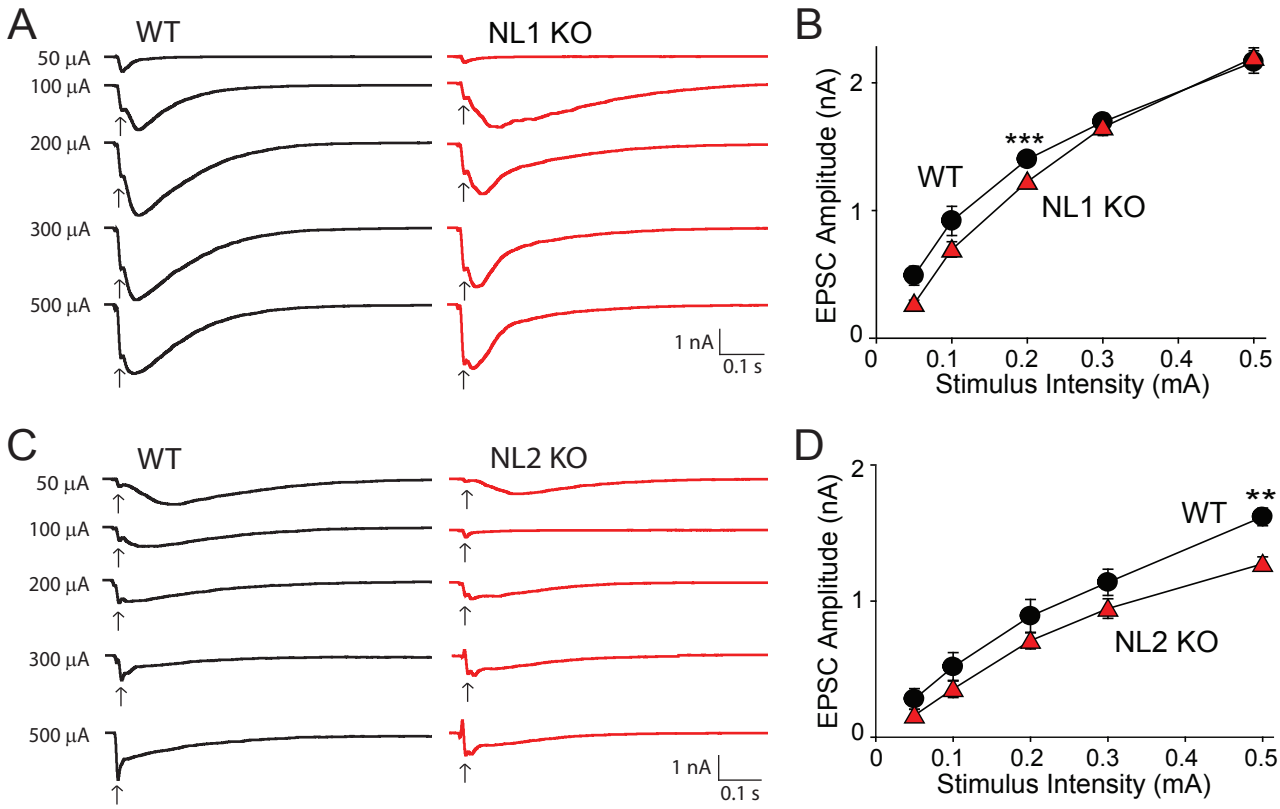

Suppl. Figure 4
Chubykin et al.

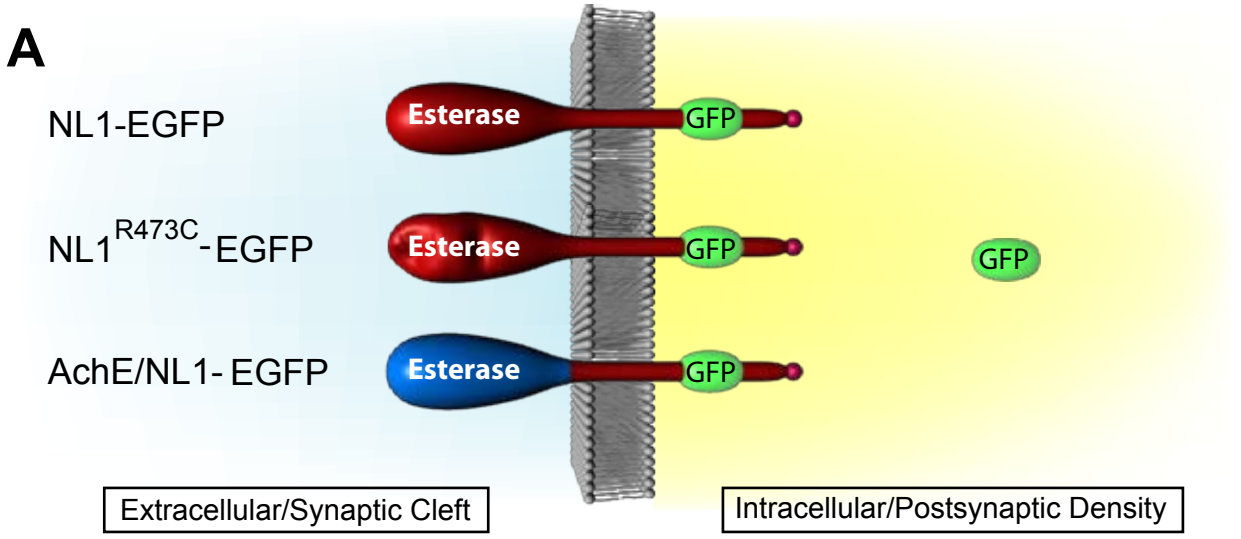

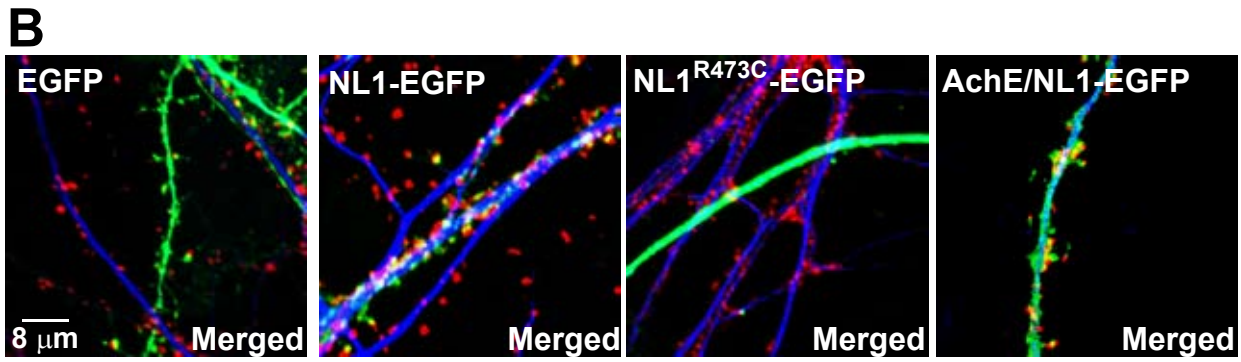

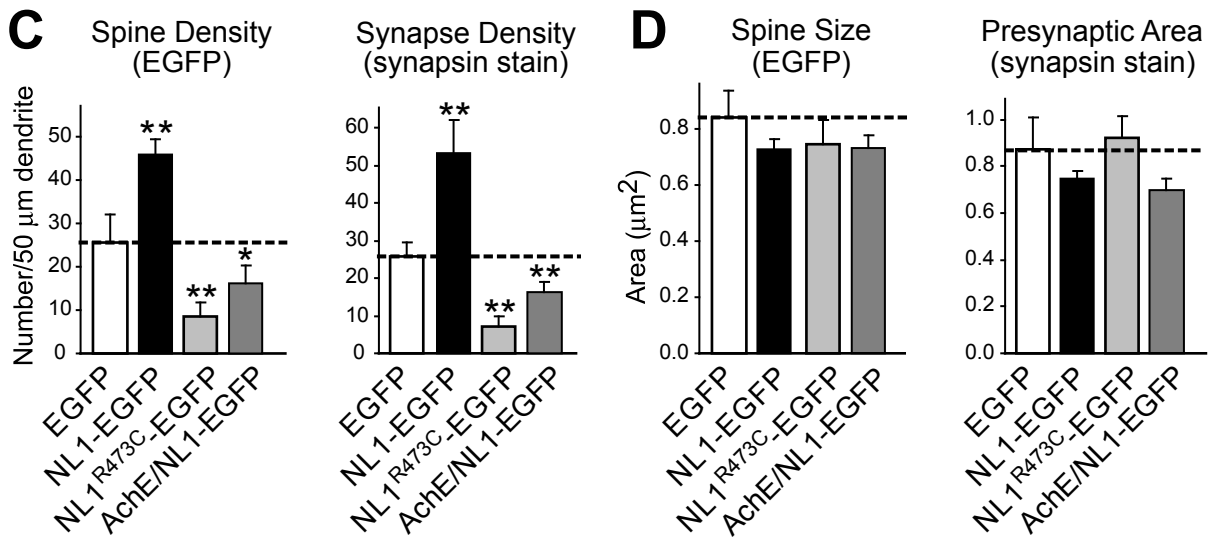

Supplementary Fig. 5
Chubykin et al.

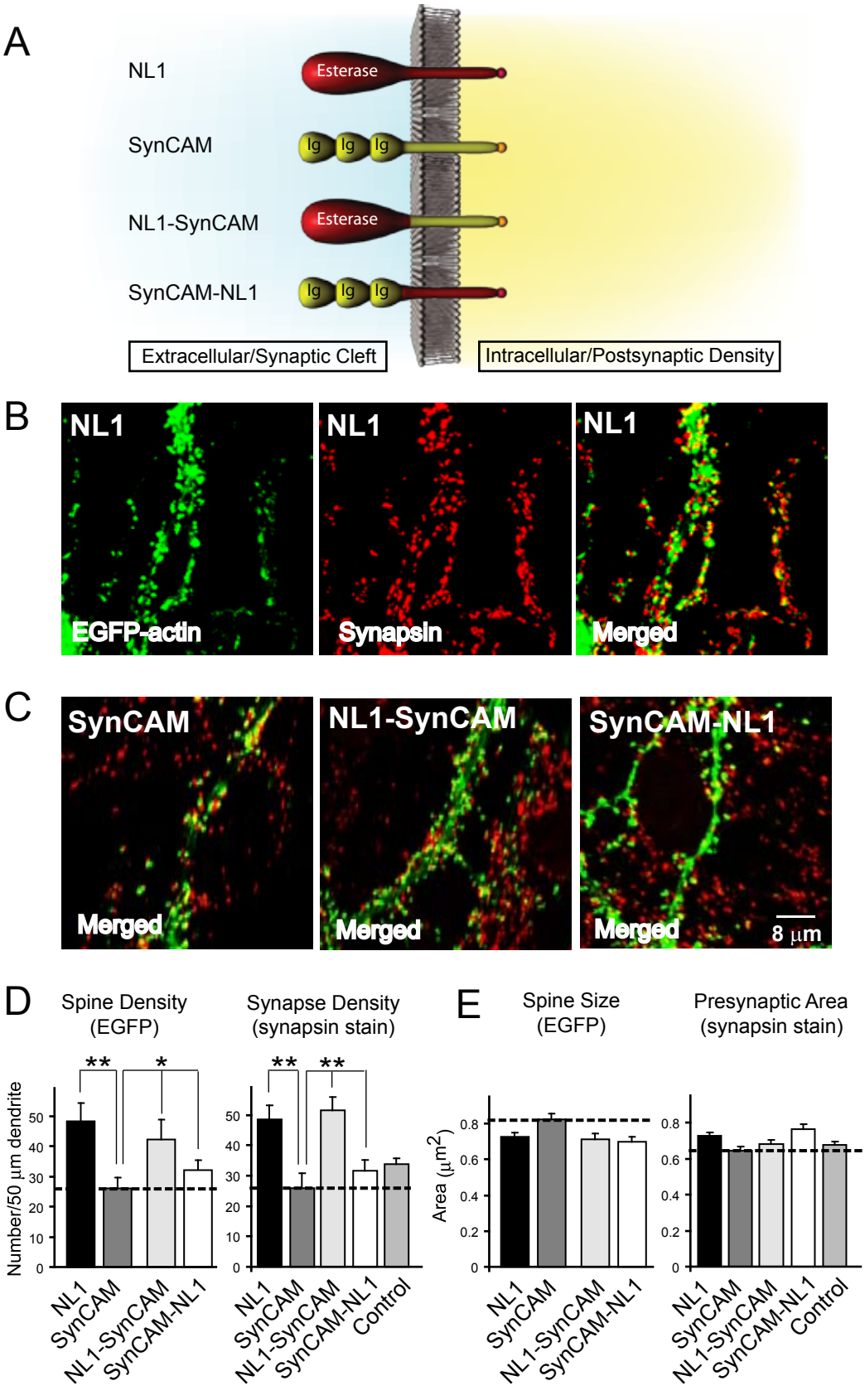

Supplementary Fig. 6
Chubykin et al.

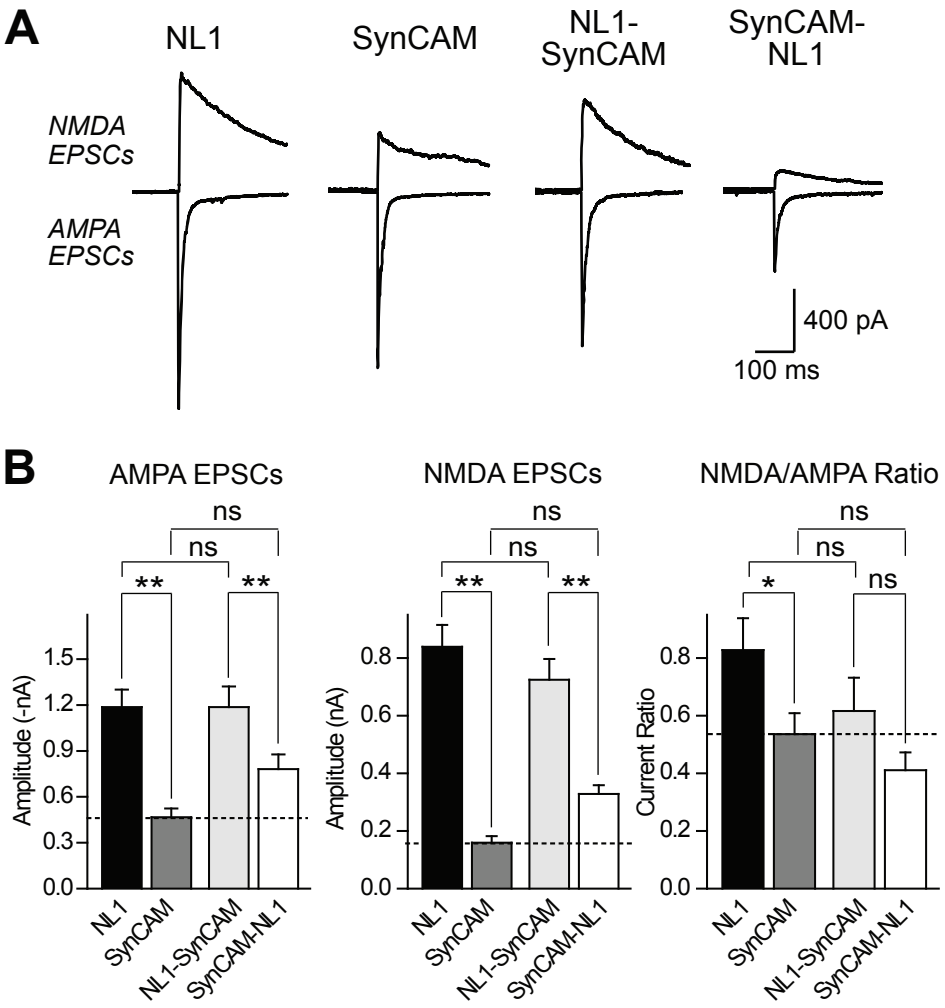

Supplementary Fig. 7
Chubykin et al.

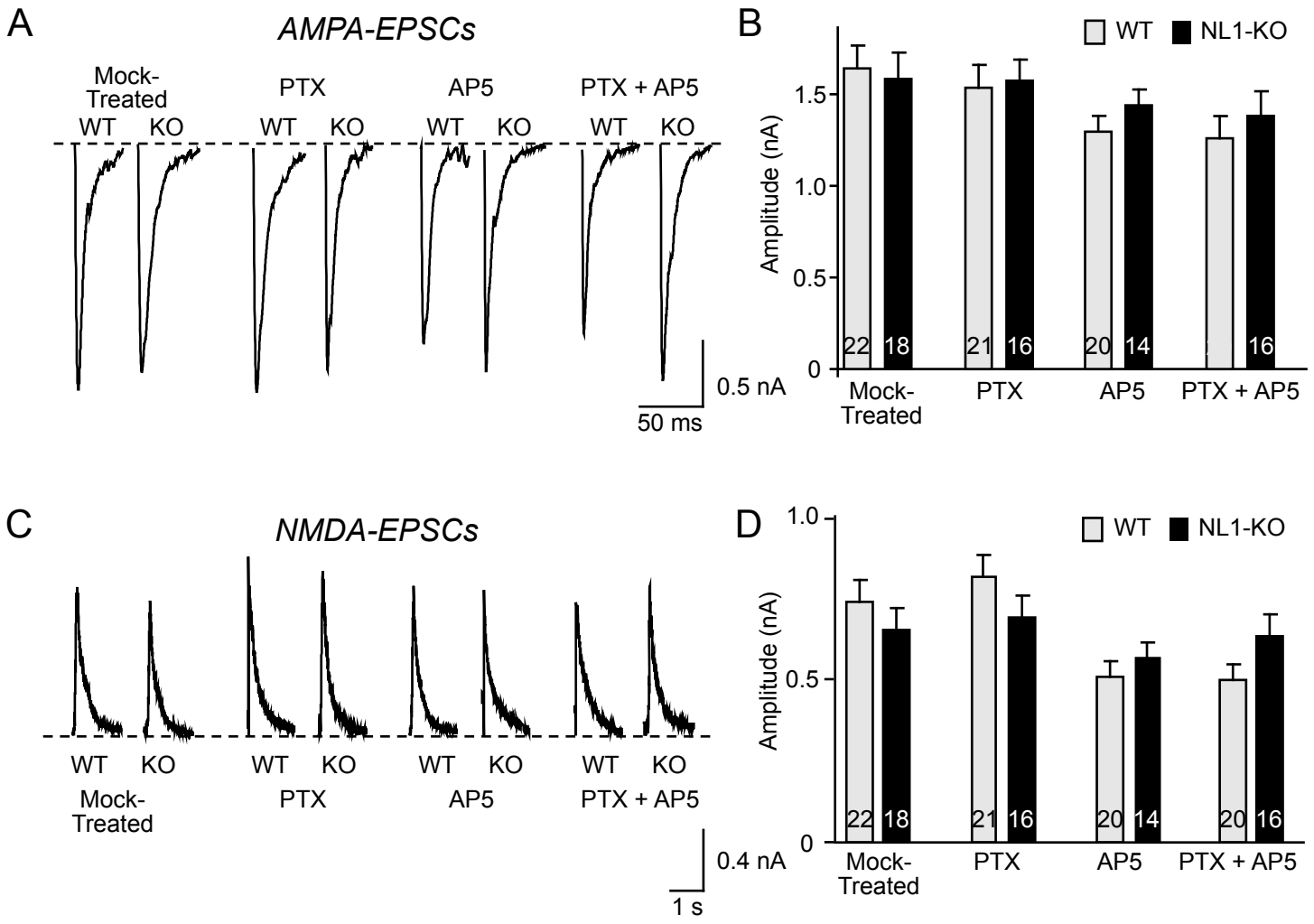

Suppl. Figure 8
Chubykin et al.